frontiers in Energy Research

ORIGINAL RESEARCH
published: 26 April 2021
doi: 10.3389/fenrg.2021.643431

Sulfur Poisoning and Performance Recovery of SOFC Air Electrodes

*Junsung Hong†, M. R. Anisur, Su Jeong Heo†, Pawan Kumar Dubey and Prabhakar Singh**

Department of Materials Science and Engineering, University of Connecticut, Storrs, CT, United States

OPEN ACCESS

Edited by:
Zafar Said,
University of Sharjah, United Arab Emirates

Reviewed by:
Miguel A. Laguna-Bercero,
University of Zaragoza, Spain
Daniel Araújo de Macedo,
Federal University of Paraíba, Brazil
Stephen Skinner,
Imperial College London, United Kingdom

***Correspondence:**
Prabhakar Singh
prabhakar.singh@uconn.edu

†Present address:
Junsung Hong,
Department of Materials Science and Engineering, Northwestern University, Evanston, IL, United States
Su Jeong Heo,
Materials Science Center, National Renewable Energy Laboratory, Golden, CO, United States

Specialty section:
This article was submitted to Fuel Cells, a section of the journal Frontiers in Energy Research

Received: *18 December 2020*
Accepted: *04 March 2021*
Published: *26 April 2021*

Citation:
Hong J, Anisur MR, Heo SJ, Dubey PK and Singh P (2021) Sulfur Poisoning and Performance Recovery of SOFC Air Electrodes. Front. Energy Res. 9:643431. doi: 10.3389/fenrg.2021.643431

The sulfur poisoning and performance recovery of the state-of-the-art SOFC cathodes $(La_{0.80}Sr_{0.20})_{0.95}MnO_{3\pm\delta}$ (LSM) and $(La_{0.60}Sr_{0.40})_{0.95}Co_{0.20}Fe_{0.80}O_{3-\delta}$ (LSCF), have been studied. Electrochemical impedance spectroscopy measurements of LSCF|GDC and LSM|YSZ half-cells are carried out in alternating atmospheres of air and SO_2–air at 700°C for hundreds of hours. In the presence of SO_2, the electrochemical performance of both the cells decays with ohmic and non-ohmic losses, owing to the absorption and chemical interaction of SO_2 with the electrodes. In LSCF, the SrO segregated on the surface tends to absorb and react with SO_2, forming $SrSO_4$ followed by the exsolution of Co-Fe. As for LSM, SO_2 is absorbed onto the Sr-rich areas of LSM, including the active reaction sites near the TPBs, leading to Sr exsolution and $SrSO_4$ formation, leaving a Sr-deficient LSM. During the subsequent exposure to air, the performance of the sulfur-contaminated LSM is almost restored. The LSM particles, exposed to alternating atmospheres of air and SO_2-air during the electrochemical tests, show a relatively clean surface with sparsely distributed $SrSO_4$ particles, indicating a high stability against sulfur poisoning. It is suggested that the loosely adsorbed SO_2 at the TPBs is readily swept away by the SO_2-free air flow, recovering its ORR activity, whereas the Sr-deficient LSM due to Sr-exsolution stays modified, contributing to the incomplete performance restoration. Unlike the case of LSM, the performance of the sulfur-poisoned LSCF partially recovers during the subsequent exposure to air. Correspondingly, the LSCF particles have a modified morphology covered with numerous nanoparticles, mostly $SrSO_4$, showing the irreversible aspect of the sulfur poisoning. The morphology modification is not concentrated near the electrode/electrolyte interface but over the entire cathode, indicating that the degree of recovery from sulfur poisoning is closely related to the presence of SrO and chemical activity of Sr in the electrodes at the solid-gas interface. These results also show the potential application of LSM for a sulfur sensor available in high-temperature harsh conditions.

Keywords: sulfur poisoning, performance recovery, solid oxide fuel cell, air-electrode, LSM, LSCF, electrochemical impedance spectroscopy, $SrSO_4$

INTRODUCTION

The need for enhancement in the efficiency and durability of solid oxide fuel cells (SOFC) has stimulated extensive research. Cathode degradation is known to account for the largest portion of the electrochemical losses during long-term SOFC operation (Yokokawa, 2015). A number of studies have reported on the fundamental understanding of SOFC cathode degradation and approaches to minimize the impact of cathode degradation (Simner et al., 2006; Liu et al., 2009, 2012; Zubair et al., 2014; Yang et al., 2017). The main causes of the cathode degradation include microstructure coarsening, phase separation, chemical interaction with electrolyte, delamination at electrode/electrolyte interfaces, and poisoning by airborne contaminants (Chen et al., 2016).

Sulfur dioxide (SO_2) is one of the commonly present representative impurities in addition to Cr vapors (Horita et al., 2009; Hong et al., 2020). Although the concentration of SO_2 is very low in air (75 ppb for hourly primary standard) (National Ambient Air Quality Standards by US Environmental Protection Agency, 2010), the long-term exposure of the cathode to air flow can lead to contaminant deposition and reaction, degrading the cathodic activity for oxygen reduction reaction (ORR) (Singh and Birks, 1978; Mori et al., 2015). Particularly, LSCF is considered vulnerable to sulfur poisoning as the surface-segregated SrO is prone to react with SO_2 forming $SrSO_4$ (Mori et al., 2015; Yu et al., 2016; De Vero et al., 2018). The airborne SO_2 also contaminates LSM electrodes, although the effect may not be as severe as on LSCF (Liu et al., 2011; Daio et al., 2016). The degradation caused by SO_2 is slow but continuous and severe in the long term. Higher concentrations of SO_2 (0.1, 1, 10, and 100 ppm) showed an accelerated degradation in the SOFC performance (Wang et al., 2020).

The effect of SO_2 on electrode performance degradation has been extensively studied experimentally by maintaining the SO_2 concentration constant during the experiments. However, under the real SOFC operating condition, the SO_2 concentration may fluctuate depending on the ambient atmospheric conditions. The irreversible or recoverable nature of the performance loss, caused by sulfur poisoning when SO_2 concentration is reduced, remains largely unknown. In this paper, we present the findings of our study on the reversibility of sulfur poisoning and recovery of the state-of-the-art air electrodes, i.e., $(La_{0.80}Sr_{0.20})_{0.95}MnO_{3\pm\delta}$ (LSM) and $(La_{0.60}Sr_{0.40})_{0.95}Co_{0.20}Fe_{0.80}O_{3-\delta}$ (LSCF), in alternating atmospheres of air and SO_2-air. Their poisoning and recovery mechanisms were elucidated by the electrochemical impedance spectroscopy (EIS) analysis. The accompanying structural evolution and the surface chemistry of LSM and LSCF during exposure to the alternating atmosphere were also investigated using the SEM, XRD, and Raman spectroscopy. The results show that the difference in performance degradation and recovery behavior of LSM and LSCF electrodes is attributed to the presence of SrO and chemical activity of Sr in the electrodes at the solid-gas interface.

MATERIALS AND METHODS

Operando Electrochemical Analysis

For electrochemical tests, electrolyte-supported solid oxide cells with LSCF and LSM electrodes were prepared (Hong et al., 2020). Gd-doped ceria (GDC; $Gd_{0.10}Ce_{0.90}O_{1.95}$; Fuelcellmaterials, United States) and yttria-stabilized zirconia (YSZ; 8 mol.% yttria; Fuelcellmaterials, United States) button electrolytes with a diameter of 25 mm were used as supports $(La_{0.60}Sr_{0.40})_{0.95}Co_{0.20}Fe_{0.80}O_{3-\delta}$ (LSCF; Fuelcellmaterials, United States) and $(La_{0.80}Sr_{0.20})_{0.95}MnO_{3\pm\delta}$ (LSM; Fuelcellmaterials, United States) inks were screen-printed on the GDC and YSZ electrolytes, respectively, followed by firing at 1,200°C for 2 h (3°C min^{-1}). The electrode areas were 0.785 cm^2 and the electrode thicknesses were ∼10 μm. The thin electrode could result in a lower performance (Barbucci et al., 2008), but it would not affect the overall trend of the results here. Pt paste (ESL Electroscience) was applied to the opposite side as a counter electrode. Each electrode surface was attached to the Pt mesh as a current collector. The as-prepared LSCF|GDC|Pt and LSM|YSZ|Pt cells were mounted on alumina tubes with an alumina paste (Zircar Ceramics Inc., United States). A type-K thermocouple was set up close to the cell to monitor and read the exposure temperature accurately. The mounted cells were electrically connected to a potentiostat (VMP3, Bio-Logic, France). An alumina cap was placed over the assemblage to seal the whole assemblage. For details, refer to Ref. (Heo et al., 2019; Hong, 2020). The cell assembly was subsequently inserted in a furnace and heated up at 700°C (3°C min^{-1}). The electrochemical impedance spectroscopy (EIS) spectra, as well as the current change, were recorded under a bias of 0.5 V in the frequency range of 0.5 Hz to 200 kHz with a 10 mV sinus amplitude at an interval of 1 h. During the measurement, air (Ultra zero grade; 2 ppm H_2O; Airgas, Inc.) and 4 ppm SO_2 (air balance; <3 ppm H_2O) were alternately supplied to the air-electrode side at 120 mL min^{-1}, for which 10 ppm SO_2 (air balance; <3 ppm H_2O; Airgas, Inc.) and air (Ultra zero grade; 2 ppm H_2O; Airgas, Inc.) gases were blended using a gas mixing system (Series 4000, Environics, United States), while air was injected to the counter electrode side at 120 mL min^{-1}. The recorded impedance spectra were further processed by a distribution of relaxation times (DRT) analysis (Wan et al., 2015) to better understand the physicochemical process on electrodes.

Characterization

The cross sections of the LSCF/GDC and LSM/YSZ cells, which were exposed to alternating atmospheres of 4 ppm SO_2 and air during the electrochemical test, were observed and analyzed using the field-emission scanning electron microscopy (FE-SEM; Quanta 250 FEG, FEI, United States) equipped with energy dispersive X-ray spectrometry (EDS). Furthermore, LSCF and LSM, layered on YSZ substrates, were exposed to alternating atmospheres of 1 ppm SO_2 (air balance) and air at 700°C for 400 h. Their structural changes were then investigated using the SEM, Raman spectroscopy (Ramanscope 2000, Renishaw, Gloucestershire, United Kingdom) with a laser of 514.5 nm

wavelength, and X-ray diffractometer (XRD; D8 Advance, Bruker, Germany) with Cu Kα radiation (λ = 0.1542 nm).

RESULTS

EIS Study of Sulfur Poisoning and Recovery of LSM and LSCF

Total, ohmic, and polarization resistances of LSCF|GDC and LSM|YSZ half cells at 700°C in alternating atmospheres of air and 4 ppm SO_2 are displayed in **Figure 1**. Their corresponding impedance spectra are exhibited in **Figures 2**, **3**. For the LSCF|GDC cell, the resistance is initially constant in air (**Figure 1A**: 0–36 h) while the impedance spectra remain constant (**Figure 2A**: 1–30 h). As SO_2 gas (4 ppm; air balance) is supplied to the LSCF electrode (at 36 h), the impedance arcs are enlarged and the high-frequency *x*-intercept shifts to the right (**Figure 2A**: 1–50 h), indicating the increase in the polarization (R_p) and ohmic (R_Ω) resistances, respectively.

The continuous exposure of the LSCF electrode to SO_2 further degrades the electrochemical performance; both the ohmic and polarization resistances continue to increase (**Figure 1A**: 36–213 h; and **Figure 2B**: 50–213 h), indicating the vulnerability of LSCF to SO_2. For a deeper understanding of the physicochemical process during sulfur poisoning and recovery, DRT transformation is performed. DRT analysis has been frequently used, especially in SOFCs, for EIS data interpretation as it allows for deconvolution in a simple way (Wan et al., 2015), compared with the conventional non-linear least square fitting that requires an accurate equivalent circuit model. **Figure 4** shows the DRT spectra composed of four main signals (denoted as P1–P4) at different frequency ranges. For LSCF exposed to SO_2 (**Figure 4A**), all four signals increase overall. In particular, the rise of the low-frequency signal at 10^{-2}–10^{0} Hz (P4) is remarkable. This indicates the occurrence of physi- and chemisorption of SO_2 on the LSCF surface, inhibiting the catalytic activity for oxygen reduction reaction (ORR), given that the low-frequency response (<1 Hz) is related to O_2 adsorption, reduction, and dissociation into O^{2-} on air-electrodes (Yang et al., 2000, 2001; Adler, 2004). The increase of high-frequency signal at $>10^{4}$ Hz (P1) is also noticed, which is associated with oxygen ion transport at the cathode/electrolyte interface. The sulfur absorption would lead to $SrSO_4$ formation and subsequently to Co-Fe exsolution (Wang et al., 2013; De Vero et al., 2018; Budiman et al., 2019).

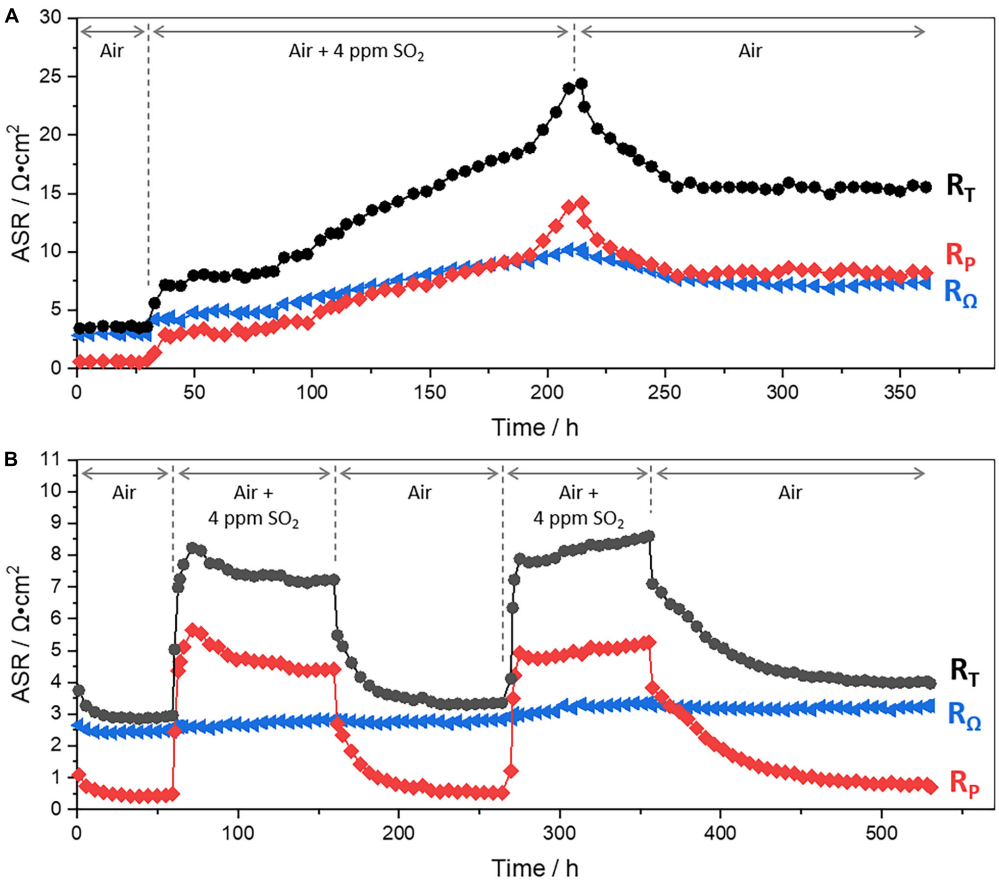

FIGURE 1 | Ohmic, polarization, and total resistances (R_Ω, R_P, and R_T, respectively) of **(A)** LSCF|GDC half-cell for ~360 h at 700°C in alternating atmospheres of air (0–36 h and 215–358 h) and 4 ppm $SO_{2(g)}$ (air balance) (36–215 h), and those of **(B)** LSM|YSZ half-cell for ~530 h at 700°C in alternating atmospheres of air (0–60, 159–268, and 354–528 h) and 4 ppm $SO_{2(g)}$ (air balance) (60–159 and 268–354 h). The corresponding current densities are displayed in **Supplementary Figure 1**.

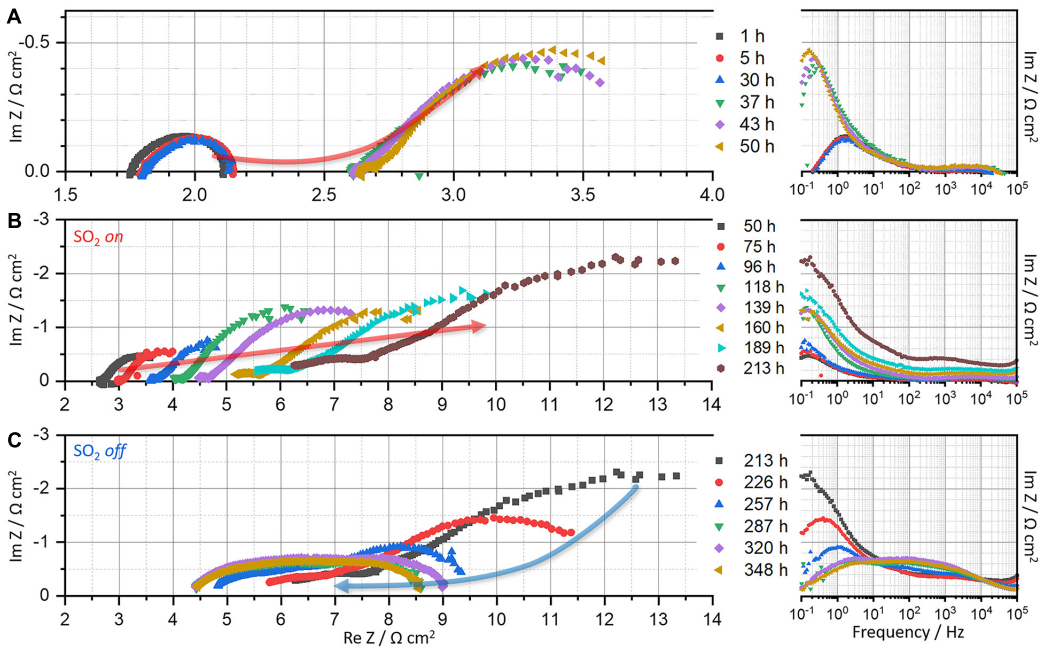

FIGURE 2 | Nyquist and bode plots of LSCF|GDC|Pt cell measured for ~360 h at 700°C in alternating atmospheres of air (0–36 and 215–358 h) and 4 ppm $SO_{2(g)}$ (36–215 h): **(A)** 1–50 h, **(B)** 50–213 h, and **(C)** 213–348 h.

Such structural change near the LSCF/GDC interface is known to switch and elongate the ionic transport pathways, increasing the high-frequency resistance (P1 or R_Ω) (Wang F. et al., 2016).

The reversibility of sulfur poisoning and recovery for LSCF is then explored, for which the SO_2 gas flow is switched back to air. Immediately after the air flow, the resistance decreases back, but just slightly (**Figure 1A**: >213 h). Noticeable changes are found in the Nyquist plots (**Figure 2C**: 213–348 h). The Nyquist arcs shift to the left and shrink over time, indicating the decrease in both ohmic and polarization resistances, respectively. DRT analysis in **Figure 4B** shows that both the low- and high-frequency components at 10^{-2}–10^{0} and $>10^{4}$ Hz (P1 and P4) largely decrease, whereas the intermediate frequency components at 10^{-2}–10^{4} Hz (P2 and P3) remain relatively unchanged. In principle, the low- and mid-frequency impedances are associated with the surface diffusion of adsorbed oxygen and the bulk diffusion of oxygen ions in air-electrodes, respectively, while the high-frequency impedance is related to the oxygen ion transfer through electrolytes (Adler et al., 1996; Yang et al., 2000, 2001; Adler, 2004; Lang et al., 2008; Nielsen and Hjelm, 2014). It is suggested that the surface LSCF structure, modified by sulfur incorporation, partially returns to its original structure in flowing air, which may include the desorption of SO_2 from LSCF and partial dissolution of exsolved $(Co,Fe)O_x$. The modified bulk structure, however, is not restored as identified by the comparison of the Nyquist curves before and after the recovery process (see superimposed curves in **Supplementary Figure 2B**). Further discussion is presented in the following section with a surface morphological analysis performed by SEM.

As for the LSM|YSZ cell, the resistances (R_Ω, R_P, and R_T) decrease for the first 30 h and then becomes constant in air (**Figure 1B**: 0–58 h) while the corresponding Nyquist curve shrinks and shifts to the left (**Figure 3A**), indicating the electrode activation and stabilization. The SO_2 gas (4 ppm; air balance) is then fed to the LSM electrode at 59 h for sulfur poisoning. As a result, the polarization resistance soars (**Figure 1B**: 58–158 h) while the Nyquist arc is enlarged (**Figure 3B**: 58–158 h). These would be caused by SO_2 adsorption on the LSM electrode surface. As the active sites for ORR and oxygen ion transfer in LSM are concentrated at triple phase boundaries (TPBs) between air, electrolyte, and electrode (Gong et al., 2012; Huber et al., 2014; Pakalapati et al., 2014), it is considered that the area contaminated with SO_2 includes the LSM near the TPBs. Unlike the case of LSCF, the ohmic resistance is not affected by SO_2 exposure and the polarization resistance no longer increases after the initial ascent within ~35 h (58–93 h), thus implying the chemical stability of LSM electrode to $SO_{2\ (g)}$.

The reversibility of sulfur poisoning and recovery for LSM is also investigated, for which the supplied $SO_{2\ (g)}$ is replaced by air. Immediately after air flow, the polarization resistance is reduced, eventually being close to its initial value, ~0.5 **Ω** cm^2 (**Figure 1B**: 158–266 h, and **Figure 3C**: 158–266 h), which indicates the recovery of the electrochemical performance of the LSM|YSZ cell. DRT plots in **Figures 4C,D** show the same trend for the restoration. The signals (P1–P3), which were increased in the presence of SO_2, are reduced in the absence of SO_2 and returned to their original levels. As with the first cyclic test, the electrochemical performance, secondarily degraded by sulfur poisoning (**Figure 3D**: 266–353 h), is restored again in

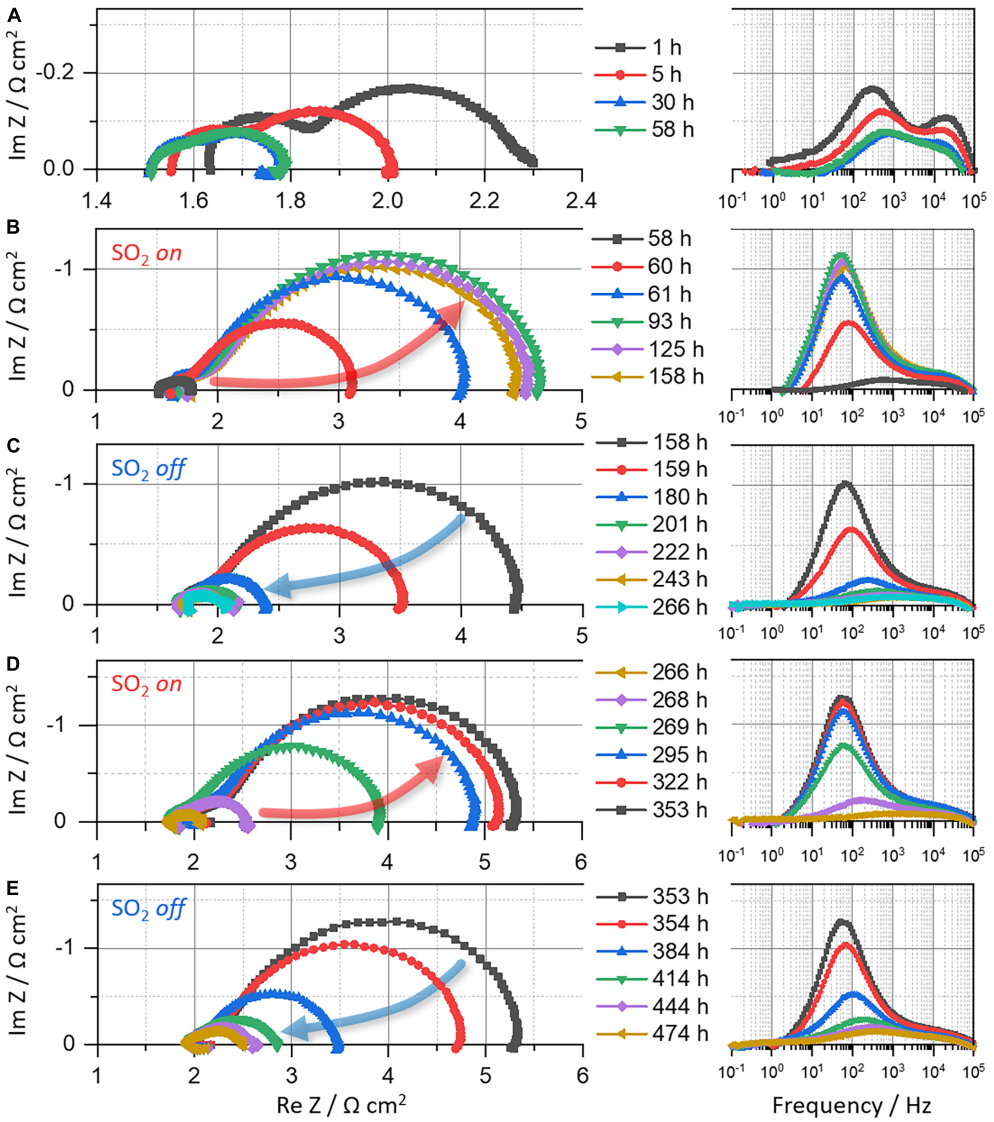

FIGURE 3 | Nyquist and bode plots of LSM|YSZ|Pt cell measured for ~530 h at 700°C in alternating atmospheres of air (1–58, 158–266, and 353–474 h) and 4 ppm $SO_{2(g)}$ (58–158 and 266–353 h): **(A)** 1–58 h, **(B)** 58–158 h, **(C)** 158–266 h, **(D)** 266–353 h, and **(E)** 353–474 h.

airflow (**Figure 3E**: 353–474 h). The observations confirm that, for sulfur-poisoned LSM, the performance recovery is almost reversible. The original and recovered impedance plots (58 and 266 h) are displayed in **Supplementary Figure 2A** for comparison. It appears that the high-frequency x-intercept (R_Ω) is shifted by 0.23 Ω cm^2 (from 1.51 to 1.74 Ω cm^2) whereas the impedance arc diameter (R_p) is rarely changed (from 0.27 to 0.34 Ω cm^2). The R_Ω increase could be attributed to the formation of poorly conductive secondary phases such as $SrSO_4$ on the LSM surface and $La_2Zr_2O_7$ at the electrode/electrolyte interface (Mitterdorfer and Gauckler, 1998; Chen et al., 2009, 2010). It is also observed that a very small impedance arc in the low-frequency range (10^0–10^1 Hz) was formed, which is likely to contribute to the R_p increase (**Supplementary Figure 2A**). As the low-frequency impedance is related to oxygen adsorption and diffusion near the surface, the LSM surface modified by sulfur poisoning may affect the slight increase in R_p. The above predictions from EIS results will be verified by post-test characterization in the following section.

Structural Modification of LSCF and LSM in Cyclic Conditions

Figure 5 shows SEM images of the cross section of LSCF|GDC cell exposed to alternating atmospheres of air and 4 ppm $SO_{2(g)}$ for ~360 h during the electrochemical test. The nanostructure of LSCF appears to change significantly. The LSCF particle surface has numerous nano-bumps indicative of Sr exsolution (**Figure 5A**), which was not initially present (**Figure 6B**). The nano-bumps are likely to be sulfur compounds such as $SrSO_4$,

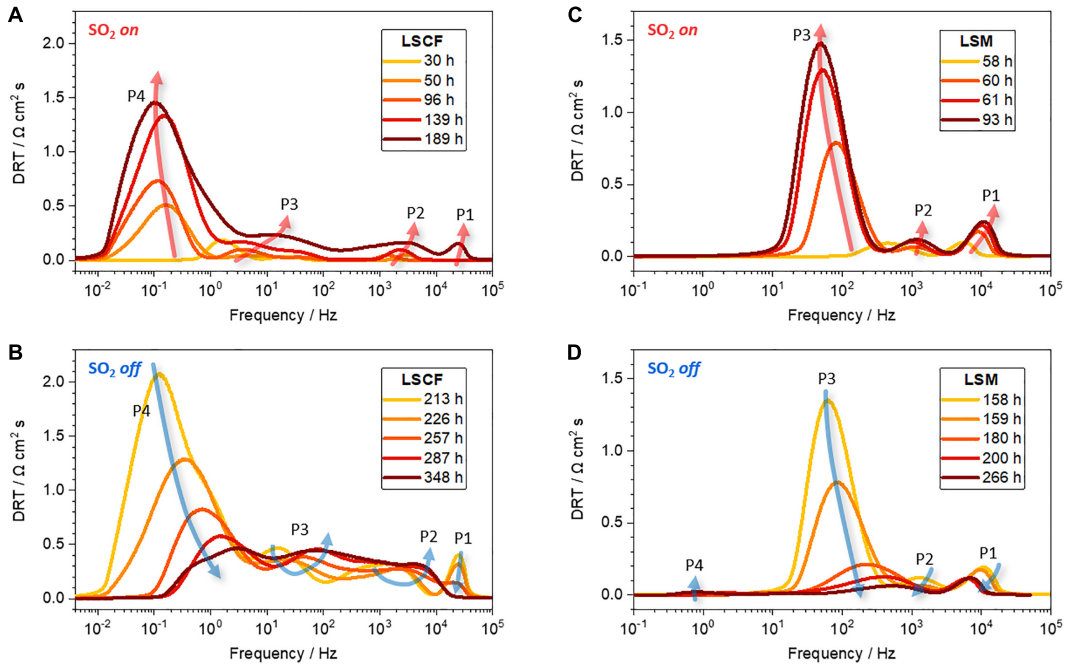

FIGURE 4 | DRT plots of the EIS spectra of **(A,B)** LSCF|GDC and **(C,D)** LSM|YSZ half-cells exposed to alternating atmospheres of air and 4 ppm $SO_{2(g)}$.

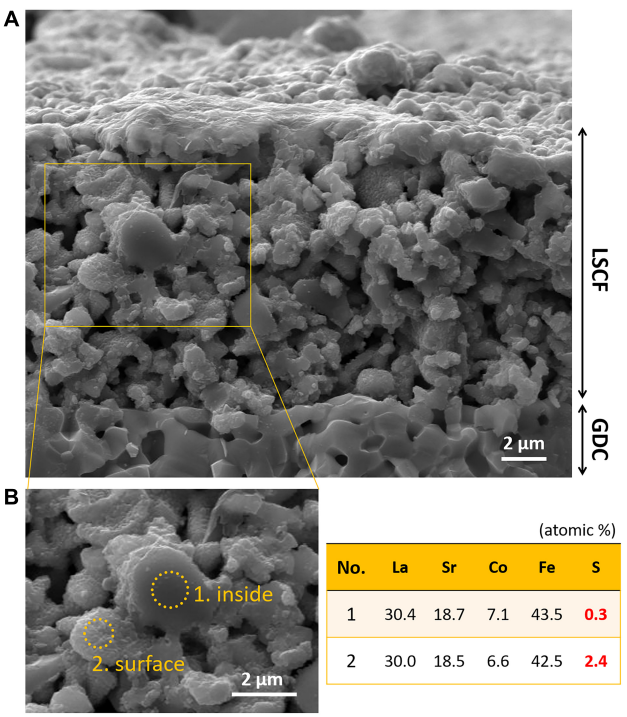

(atomic %)

No.	La	Sr	Co	Fe	S
1	30.4	18.7	7.1	43.5	0.3
2	30.0	18.5	6.6	42.5	2.4

FIGURE 5 | (A) SEM image of the cross section of the LSCF/GDC cell exposed to an alternating atmosphere of air and 4 ppm $SO_{2(g)}$ for ~360 h at 700°C during the electrochemical test. **(B)** Elemental composition (La, Sr, Co, Fe, and S) of LSCF particles measured by EDS (on the core and surface).

based on previous research (Hong et al., 2019). Correspondingly, as can be seen in **Figure 5B**, the EDS spectrum from the LSCF particle with the surface nanoparticles (Region 2), shows a higher sulfur concentration than that from the LSCF particle core (Region 1). The $SrSO_4$ formation can lead to Co/Fe exsolution, for example, $CoFe_2O_4$ formation (Wang et al., 2013; De Vero et al., 2018; Budiman et al., 2019). Indeed, the Raman analysis identifies a characteristic peak for the Co_3O_4 phase (Na et al., 2012), from a LSCF specimen that was exposed to alternating atmospheres of air and 1 ppm SO_4 (**Figure 7B**), further discussion of which will be presented below. Such structural changes are well agreed with the electrochemical performance degradation shown in **Figures 1**, **2**. Therefore, it is indicated that the LSCF structure, once modified by sulfur poisoning, cannot be structurally recovered in air flow.

Figure 8 shows the morphology of the fractured cross section of LSM|YSZ cell, which was exposed to alternating atmospheres of air and 4 ppm $SO_{2(g)}$ for ~530 h during the electrochemical test. The LSM particles appear to have smooth surfaces with no evidence of Sr exsolution and $SrSO_4$ formation (**Figure 8A**). It should be noted that in our previous study (Hong et al., 2019), an LSM|YSZ cell, exposed to 4 ppm SO_2 for 120 h but without subsequent exposure to air flow, has sulfur-enriched nanoparticles (regarded as $SrSO_4$) protruding on the surface. It is thus indicated that, in the subsequent air flow, the sulfur physi/chemisorbed on the LSM surface is released while the strontium is partially dissolved back into LSM. This result corresponds to the electrochemical performance restoration of the LSM|YSZ cell (**Figure 3**). Even after the

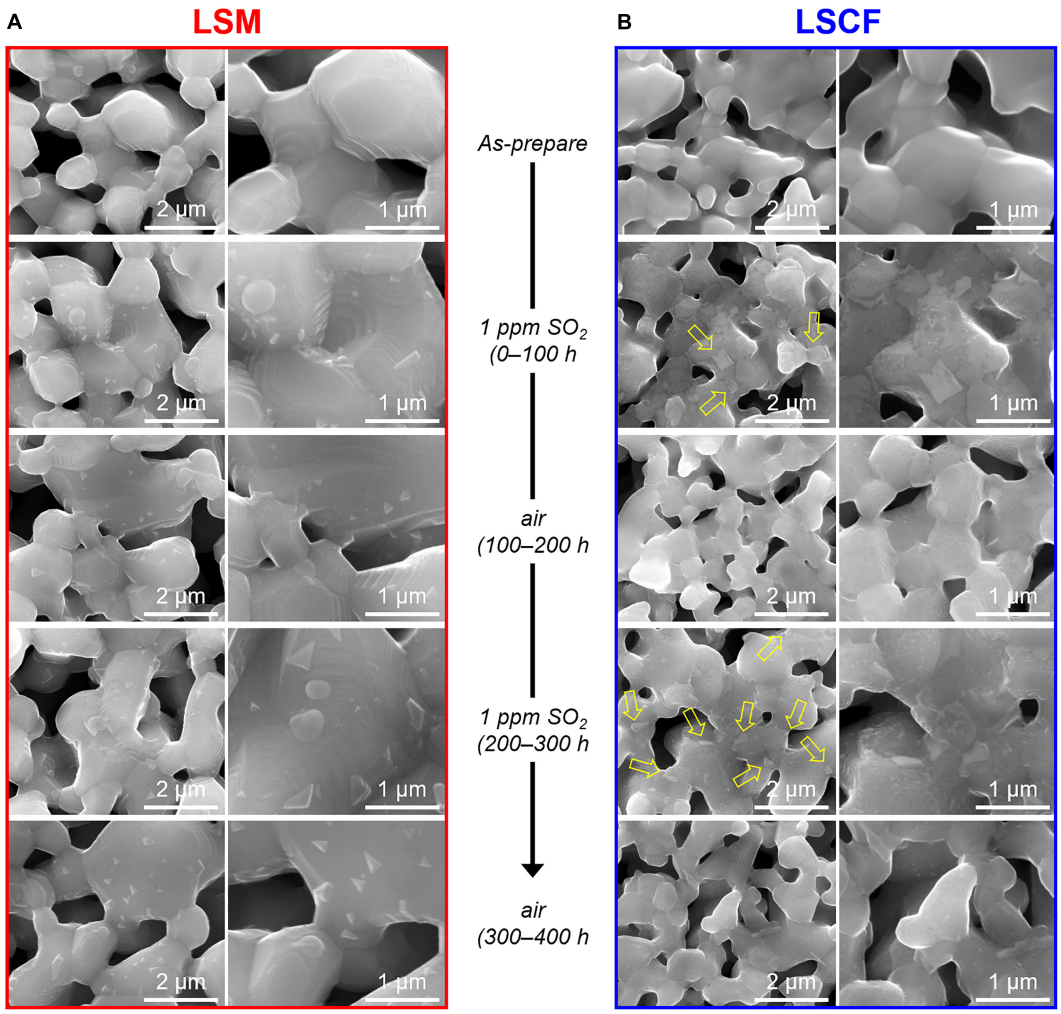

FIGURE 6 | SEM images of **(A)** LSM and **(B)** LSCF particles exposed to an alternating atmosphere of air and 1 ppm SO_2 (air balance) for 400 h at 700°C.

recovery process, however, a few particles appear to have a different morphology such as cylindrical columns (**Figure 8B**), which contain a higher concentration of sulfur than the granular particles (see the elemental compositions of three selected regions of the LSM electrode, tabulated in the inset of **Figure 8B**). Such irreversible morphology change could be the cause of the incomplete recovery of the electrochemical performance of LSM (**Supplementary Figure 2A**). When the partial pressure of SO_2 is as low as 75 ppb [in ambient air; primary standard (National Ambient Air Quality Standards by US Environmental Protection Agency, 2010)], though, the sulfur poisoning and recovery might be a completely reversible process.

To further understand the restoration of the electrochemical performance of sulfur-contaminated LSM and LSCF electrodes, the structural evolution of LSM and LSCF, exposed to alternating atmospheres of 1 ppm SO_2 (air balance) and air at 700°C, is investigated using the SEM, XRD, and Raman spectroscopy. **Figure 6** shows the nanostructure changes of LSM and LSCF during the exposure. As for LSM, nanoparticles have formed on the surface in SO_2 flow, possibly due to Sr exsolution forming $SrSO_4$ (**Figure 6A**: as-prepared, and 0–100 h). In the subsequent air flow, the number and size of the nanoparticles decreased a little but they still exist, indicating the partial dissolution of exsolved-Sr back into LSM releasing SO_2 (**Figure 6A**: 100–200 h). After the second exposure to SO_2, the nanoparticle size is enlarged, indicating further Sr exsolution (**Figure 6A**: 200–300 h). In the subsequent air flow, the particle size appears decreased but slightly bigger than that of the first cycle (**Figure 6A**: 300–400 h). However, any structural change is not found by the XRD and Raman spectroscopy as shown in **Figures 7A**, **9A**, implying that the structural change of LSM by sulfur poisoning is confined to the very surface.

In the case of LSCF, the nanostructure change associated with sulfur poisoning is more significant. In SO_2 flow, the initially smooth surface becomes rough and covered with numerous exsolved nanoparticles and angular particles [possibly $SrSO_4$ (Wang et al., 2014, 2015)], marked by arrows in **Figure 6B**: as-prepared, and 0–100 h. After subsequent exposure to air, most

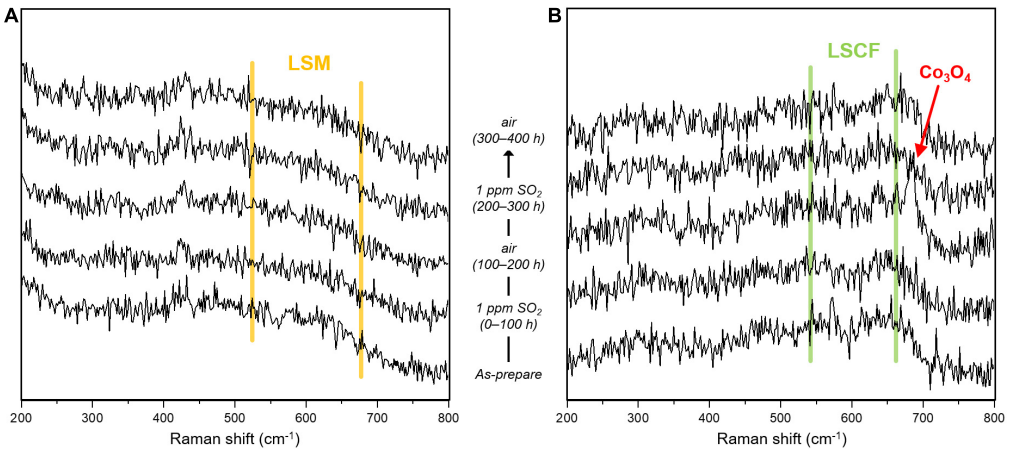

FIGURE 7 | Raman spectra of **(A)** LSM and **(B)** LSCF exposed to an alternating atmosphere of air and 1 ppm SO_2 (air balance) for 400 h at 700°C.

of the angular particles disappeared, but the surface remains still rough (**Figure 6B**: 100–200 h). It is indicated that the surface $SrSO_4$ could be partially decomposed in air flow while the strontium dissolves into LSCF. When the LSCF is again exposed to the alternating atmosphere, the same changes occur in the nanostructure (**Figure 6B**: 200–300 and 300–400 h). However, the structural change for sulfur poisoning and recovery in LSCF is not a reversible process, based on the electrochemical test results in **Figures 1A**, **2**. The irreversible process could be due to the phase separation of LSCF, for instance, Co/Fe exsolution subsequent to $SrSO_4$ formation (Cai et al., 2012; Wang et al., 2013). Raman spectroscopy identifies a characteristic peak at ~685 cm^{-1} (**Figure 7B**) corresponding to an octahedral vibration mode (A_{1g}) of Co_3O_4 phase (Na et al., 2012), indicative of Co(Fe) exsolution. In the case of Co_3O_4 phase in LSCF, similar to other studies (Upasen et al., 2015; Li et al., 2018), only the signal for A_{1g} mode is distinctive over the other four Raman modes at 190.8 (F_{2g}), 478.6 (E_g), 519.2 (F_{2g}), and 616.6 (F_{2g}) of Co_3O_4, which may be attributed to a spinel-type Co/Fe oxide formation (Benson et al., 1999; Diallo et al., 2015). Correspondingly, the doublet peaks at around 40°, 58°, and 68° for perovskite LSCF in the XRD patterns are slightly modified in the intensity over time (**Figure 9B**). This is indicative of Sr/Co/Fe exsolution because a decreasing strontium content can cause [Co(Fe)O_6] octahedra distortion and lattice structure transformation from pseudo-cubic to rhombohedral (Deganello et al., 2007; Guo et al., 2021).

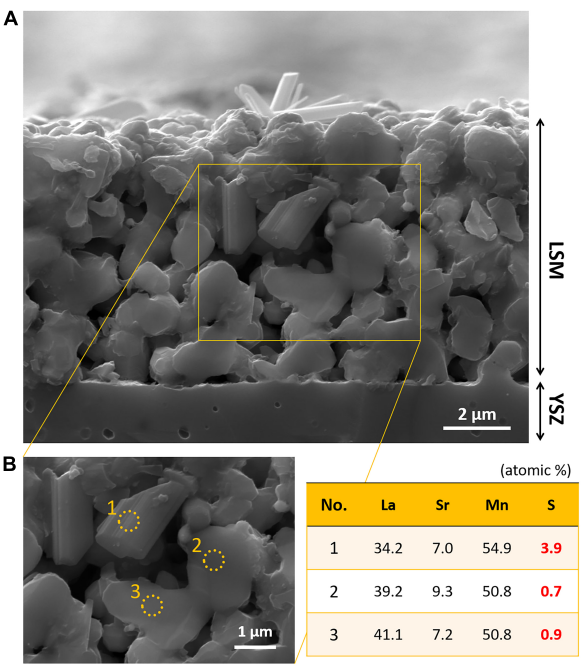

No.	La	Sr	Mn	S
1	34.2	7.0	54.9	3.9
2	39.2	9.3	50.8	0.7
3	41.1	7.2	50.8	0.9

FIGURE 8 | (A) SEM image of the cross section of the LSM/YSZ cell exposed to an alternating atmosphere of air and 4 ppm $SO_{2(g)}$ for ~530 h at 700°C during the electrochemical test. **(B)** Elemental composition (La, Sr, Mn, and S) of LSM particles measured by EDS (on the core and surface).

DISCUSSION

The experimental findings show two different behaviors of the electrochemical performance degradation and recovery of LSCF and LSM electrodes in the alternating atmospheres of air and SO_2-air at 700°C. Particularly for LSM, the performance degradation due to sulfur poisoning was almost completely restored in the subsequent air flow, whereas the performance deterioration of LSCF partially recovered, indicating the high stability of LSM to SO_2 contaminant. Electrochemical and post-test characterizations elucidate the sulfur poisoning and recovery process.

Figures 10A–C illustrates a schematic diagram of the process of sulfur poisoning and recovery for the LSCF electrode. Basically, for LSCF at high temperatures (>500°C), strontium tends to exsolve from the A-site of perovskite LSCF, forming SrO on the surface (**Figure 10A**; Lee et al., 2013; Koo et al., 2018). Because of the high affinity of SrO with $SO_{2(g)}$, the

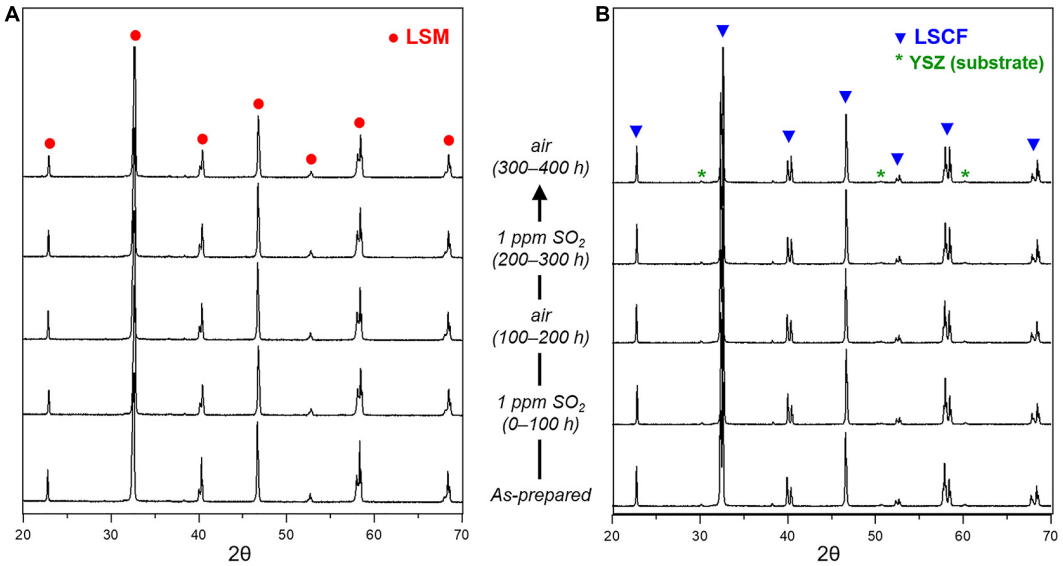

FIGURE 9 | X-ray diffraction patterns of **(A)** LSM and **(B)** LSCF exposed to an alternating atmosphere of air and 1 ppm SO_2 (air balance) for 400 h at 700°C, where YSZ was used as a substrate to support the thin LSM and LSCF layers.

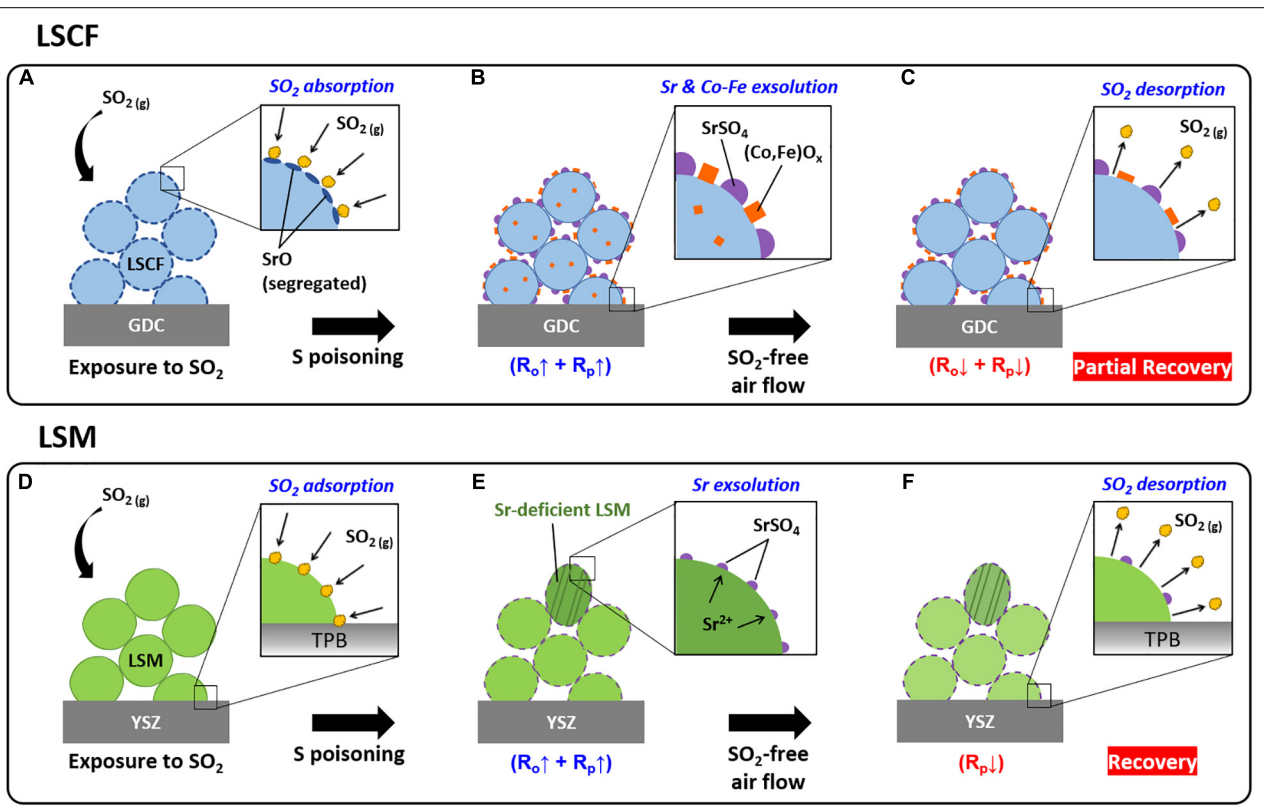

FIGURE 10 | Schematic diagram of the sulfur poisoning and recovery process of the LSCF and LSM electrodes under the presence and absence of $SO_{2(g)}$: **(A)** SO_2 absorption at SrO present on the LSCF particle surface, **(B)** $SrSO_4$ formation and Co-Fe exsolution over LSCF, **(C)** SO_2 desorption and partial dissolution of $SrSO_4$ and $(Co,Fe)O_x$ onto LSCF under SO_2-free air flow, **(D)** SO_2 absorption on the Sr-terminated LSM particle surface, **(E)** $SrSO_4$ island formation on the LSM surface leaving a Sr-deficient LSM, and **(F)** SO_2 desorption and partial dissolution of $SrSO_4$ onto LSM under SO_2-free air flow.

SrO on the surface absorbs and reacts with airborne SO_2, forming $SrSO_4$ (**Figure 10B**). The $SrSO_4$ covering the LSCF surface interferes with oxygen reduction reaction at the surface, increasing polarization resistance (R_p). The $SrSO_4$ formation leads to the loss of Sr in (La,Sr)(Co,Fe)O_3 perovskite and thereby the segregation of Co and Fe, such as the exsolution of Co_3O_4 (**Figure 7B**) and $CoFe_2O_4$ (Wang et al., 2013; De Vero et al., 2018; Budiman et al., 2019). This phase separation of LSCF (LSCF→LSCF + $SrSO_4$ + $CoFe_2O_4$) could reduce the electric conductivity and/or increase the length of oxygen diffusion path, thereby increasing the ohmic resistance (R_Ω) as well as the polarization resistance (R_p) (**Figure 10C**). When the sulfur-contaminated LSCF is subsequently exposed to air flow, the SO_2 absorbed on the LSCF and incorporated in $SrSO_4$ could be partially released out, whereas the exsolved Co and Fe in each LSCF particle is unlikely to be dissolved back into LSCF at the relatively low operating temperature (700°C), resulting in the incomplete performance recovery for LSCF. In conclusion, the recovery of the structural change and degradation by sulfur poisoning for LSCF cannot be sufficiently achieved as the sulfur poisoning significantly transforms the LSCF structure.

The process of sulfur poisoning and recovery for LSM is displayed in **Figures 10D–F**. Unlike LSCF, LSM is thermally stable without A-site cation (i.e., Sr) exsolution at high temperatures (>500°C). However, in the presence of SO_2, Sr-terminated LSM surface is likely to interact with and absorb SO_2 forming $SrSO_4$ on the top surface of the LSM particles (**Figure 10D**), which hinders the oxygen reduction reaction. Nevertheless, the Sr exsolution accompanied by $SrSO_4$ formation is localized at the surface, yielding a Sr-deficient LSM in the vicinity of the surface, but which does not cause additional structural changes of LSM (**Figure 10E**). Correspondingly, the polarization resistance (R_p) increased, whereas the ohmic resistance (R_Ω) remains as it is (**Figure 3**). When the sulfur-contaminated LSM is subsequently exposed to air, the strontium of $SrSO_4$ partially dissolves back into LSM, releasing SO_2 (including physically adsorbed SO_2) to air (**Figure 10F**). Thus, the performance degradation (mainly R_p increase) of LSM mostly recovers, although the ohmic resistance slightly increases after the poisoning and recovery process. The minor increase in the ohmic resistance could be due to the formation of a poorly conductive $SrSO_4$ on the surface and to $SrZrO_3$/$La_2Zr_2O_7$ formation by interdiffusion of La/Sr and Zr at the electrode/electrolyte interface where the latter is a natural aging process in air (Mitterdorfer and Gauckler, 1998; Chen et al., 2009, 2010; Wang C.C. et al., 2016). Considering that the SO_2 concentration (4 ppm) used in this work is much higher than the actual concentration in ambient air (75 ppb), the reversible recovery of sulfur poisoning for LSM would be achievable in general cases.

CONCLUSION

The reversibility of sulfur poisoning and recovery of the LSCF and LSM air-electrodes have been investigated. It is proposed that, for Sr-containing perovskite air-electrodes, the chemical activity of Sr is a major factor that determines the structural stability and the reversibility of the recovery of sulfur poisoning. In the presence of SO_2, the catalytic activity of the electrodes for ORR decreases along with the polarization resistance increase in low-frequency regions. For LSCF, the SrO, segregated on the LSCF surface, has a tendency to absorb and react with SO_2. Thus, LSCF electrode particles absorb airborne SO_2 forming $SrSO_4$ followed by the exsolution of Co and Fe. In the subsequent exposure to air, the electrochemical performance of LSCF does not recover as the LSCF particles predominantly remain covered with $SrSO_4$ and Co/Fe oxides (e.g., Co_3O_4) nanoparticles. In contrast, for LSM, the absorption of SO_2 is limited to the Sr-rich areas of LSM, including the active reaction sites near the TPBs, leading to a sparse Sr exsolution with $SrSO_4$ formation and Sr-deficient LSM formation. Immediately after the subsequent exposure to air, the SO_2, loosely adsorbed on the LSM surface, is easily swept away while $SrSO_4$ is partially decomposed, releasing SO_2, and dissolving Sr into the bulk LSM, by which the electrochemical performance is mostly restored. Although minor, the ohmic resistance slightly increased because of Sr-deficiency in LSM and the presence of a poorly conductive $SrSO_4$. Considering the high SO_2 concentration (4 ppm) used in this work, the reversible recovery of sulfur poisoning is achievable for LSM in ambient air. The result also shows the potential application of LSM for a sulfur sensor available in high-temperature harsh conditions.

DATA AVAILABILITY STATEMENT

The original contributions presented in the study are included in the article/**Supplementary Material**. Further inquiries can be directed to the corresponding author.

AUTHOR CONTRIBUTIONS

The results presented here are based on part of the author JH's doctoral dissertation. All authors extensively discussed the results, reviewed the manuscript, and approved the final version of the manuscript to be published.

FUNDING

This work was financially supported by a federal grant (DE-FE 0023385) from the United States Department of Energy (DOE) and National Energy Technology Laboratory (NETL).

SUPPLEMENTARY MATERIAL

The Supplementary Material for this article can be found online at: https://www.frontiersin.org/articles/10.3389/fenrg.2021.643431/full#supplementary-material

REFERENCES

Adler, S. B. (2004). Factors Governing Oxygen Reduction in Solid Oxide Fuel Cell Cathodes †. *Chem. Rev.* 104, 4791–4844. doi: 10.1021/cr020724o

Adler, S. B., Lane, J. A., and Steele, B. C. H. (1996). Electrode Kinetics of Porous Mixed-Conducting Oxygen Electrodes. *J. Electrochem. Soc.* 143, 3554–3564. doi: 10.1149/1.1837252

Barbucci, A., Carpanese, M., Reverberi, A. P., Cerisola, G., Blanes, M., Cabot, P. L., et al. (2008). Influence of electrode thickness on the performance of composite electrodes for SOFC. *J. Appl. Electrochem.* 38, 939–945. doi: 10.1007/s10800-008-9500-z

Benson, S. J., Waller, D., and Kilner, J. A. (1999). Degradation of La0. 6Sr0. 4Fe0. 8Co0. 2 O 3- δ in carbon dioxide and water atmospheres. *J. Electrochem. Soc.* 146:1305. doi: 10.1149/1.1391762

Budiman, R. A., Liu, S. S., Bagarinao, K. D., Ishiyama, T., Kishimoto, H., Yamaji, K., et al. (2019). Determination of Factors Governing Surface Composition and Degradation of La0.6Sr0.4Co0.2Fe0.8O3-δ Electrode under Sulfur-Contained Air. *J. Electrochem. Soc.* 166, F414–F422. doi: 10.1149/2.0091906jes

Cai, Z., Kubicek, M., Fleig, J., and Yildiz, B. (2012). Chemical heterogeneities on $La_{0.6}Sr_{0.4}CoO_{3-\delta}$ thin films-correlations to cathode surface activity and stability. *Chem. Mater.* 24, 1116–1127. doi: 10.1021/cm203501u

Chen, A., Smith, J. R., Duncan, K. L., DeHoff, R. T., Jones, K. S., and Wachsman, E. D. (2010). Effect of La2Zr2O7 on Interfacial Resistance in Solid Oxide Fuel Cells. *J. Electrochem. Soc.* 157:B1624. doi: 10.1149/1.3484092

Chen, M., Liu, Y. L., Hagen, A., Hendriksen, P. V., and Poulsen, F. W. (2009). LSM-YSZ reactions in different atmospheres. *Fuel Cells* 9, 833–840. doi: 10.1002/fuce.200800129

Chen, Y., Ding, D., Wei, T., and Liu, M. (2016). *Fundamental Investigations and Rational Design of Durable High-Performance SOFC Cathodes*. Atlanta, GA: Georgia Inst. of Technology.

Daio, T., Mitra, P., Lyth, S. M., and Sasaki, K. (2016). Atomic-resolution analysis of degradation phenomena in SOFCS: a case study of SO_2 poisoning in LSM cathodes. *Int. J. Hydrogen Energy* 41, 12214–12221. doi: 10.1016/j.ijhydene.2016.05.216

De Vero, J. C., Develos-Bagarinao, K., Liu, S. S., Kishimoto, H., Ishiyama, T., Yamaji, K., et al. (2018). Sulfur poisoning behavior of La1-xSrxCo1-yFeyO3-δ thin films with different compositions. *J. Alloys Compd.* 748, 608–619. doi: 10.1016/j.jallcom.2018.03.198

Deganello, F., Esposito, V., Miyayama, M., and Traversa, E. (2007). Cathode Performance of Nanostructured La 1-aSraCo1-bFebO3-x on a Ce0.8Sm0.2O2 Electrolyte Prepared by Citrate-Nitrate Autocombustion. *J. Electrochem. Soc.* 154, A89–A96. doi: 10.1149/1.2400611

Diallo, A., Beye, A. C., Doyle, T. B., Park, E., and Maaza, M. (2015). Green synthesis of Co3O4 nanoparticles via Aspalathus linearis: physical properties. *Green Chem. Lett. Rev.* 8, 30–36.

Gong, M., Gemmen, R. S., and Liu, X. (2012). Modeling of oxygen reduction mechanism for 3PB and 2PB pathways at solid oxide fuel cell cathode from multi-step charge transfer. *J. Power Sources* 201, 204–218. doi: 10.1016/j.jpowsour.2011.11.002

Guo, L., Bo, L., Li, Y., Jiang, Z., Tian, Y., and Li, X. (2021). Sr doping effect on the structure property and NO oxidation performance of dual-site doped perovskite La(Sr)Co(Fe)O3. *Solid State Sci.* 113:106519. doi: 10.1016/j.solidstatesciences.2020.106519

Heo, S. J., Hong, J., Aphale, A., Hu, B., and Singh, P. (2019). Chromium Poisoning of La1-xSrxMnO3±δ Cathodes and Electrochemical Validation of Chromium Getters in Intermediate Temperature-Solid Oxide Fuel Cells. *J. Electrochem. Soc.* 166, F990–F995.

Hong, J. (2020). *Mitigation of Air-Electrode Degradation in High-Temperature Electrochemical Systems: capture of Airborne Contaminants by Getters*. Ph. D thesis, (UCNNO: Storrs), 2021:2585.

Hong, J., Aphale, A. N., Heo, S. J., Hu, B., Reisert, M., Belko, S., et al. (2019). Strontium Manganese Oxide Getter for Capturing Airborne Cr and S Contaminants in High-Temperature Electrochemical Systems. *ACS Appl. Mater. Interf.* 11, 34878–34888. doi: 10.1021/acsami.9b09677

Hong, J., Heo, S. J., and Singh, P. (2020). Combined Cr and S poisoning behaviors of La1-xSrxMnO3±δ and La1-xSrxCo1-yFeyO3-δ cathodes in solid oxide fuel cells. *Appl. Surf. Sci.* 530:147253. doi: 10.1016/j.apsusc.2020.147253

Horita, T., Kishimoto, H., Yamaji, K., Brito, M. E., Xiong, Y., Yokokawa, H., et al. (2009). Effects of impurities on the degradation and long-term stability for solid oxide fuel cells. *J. Power Sources* 193, 194–198. doi: 10.1016/j.jpowsour.2008.10.127

Huber, T. M., Kubicek, M., Opitz, A. K., and Fleig, J. (2014). The Relevance of Different Oxygen Reduction Pathways of $La_{0.8}Sr_{0.2}MnO_3$ (LSM) Thin Film Model Electrodes. *J. Electrochem. Soc.* 162, F229–F242. doi: 10.1149/2.0061503jes

Koo, B., Kim, K., Kim, J. K., Kwon, H., Han, J. W., and Jung, W. C. (2018). Sr Segregation in Perovskite Oxides: why It Happens and How It Exists. *Joule* 2, 1476–1499. doi: 10.1016/j.joule.2018.07.016

Lang, M., Auer, C., Eismann, A., Szabo, P., and Wagner, N. (2008). Investigation of solid oxide fuel cell short stacks for mobile applications by electrochemical impedance spectroscopy. *Electrochim. Acta* 53, 7509–7513. doi: 10.1016/j.electacta.2008.04.047

Lee, W., Han, J. W., Chen, Y., Cai, Z., and Yildiz, B. (2013). Cation size mismatch and charge interactions drive dopant segregation at the surfaces of manganite perovskites. *J. Am. Chem. Soc.* 135, 7909–7925. doi: 10.1021/ja3125349

Li, J., Li, J., Yan, D., Pu, J., Chi, B., and Jian, L. (2018). Promoted Cr-poisoning tolerance of La2NiO4+ δ-coated PrBa0. 5Sr0. 5Co1. 5Fe0. 5O5+ δ cathode for intermediate temperature solid oxide fuel cells. *Electrochim. Acta* 270, 294–301.

Liu, R.-R., Taniguchi, S., Shiratori, Y., Ito, K., and Sasaki, K. (2011). Influence of SO_2 on the Long-term Durability of SOFC Cathodes. *ECS Trans.* 35, 2255–2260. doi: 10.1016/0006-291X(91)90903-K

Liu, Y. L., Hagen, A., Barfod, R., Chen, M., Wang, H. J., Poulsen, F. W., et al. (2009). Microstructural studies on degradation of interface between LSM–YSZ cathode and YSZ electrolyte in SOFCs. *Solid State Ionics* 180, 1298–1304. doi: 10.1016/j.ssi.2009.07.011

Liu, Y. L., Thydén, K., Chen, M., and Hagen, A. (2012). Microstructure degradation of LSM-YSZ cathode in SOFCs operated at various conditions. *Solid State Ionics* 206, 97–103. doi: 10.1016/j.ssi.2011.10.020

Mitterdorfer, A., and Gauckler, L. J. (1998). La2Zr2O7 formation and oxygen reduction kinetics of the La0.85Sr0.15MnyO3. O2(g)| YSZ system. *Solid State Ionics* 111, 185–218. doi: 10.1016/s0167-2738(98)00195-7

Mori, N., Sato, Y., Iha, M., Takada, T., Konoike, T., Kishimoto, H., et al. (2015). Sulfur Poisoning of LSCF Cathode in Single Step Co-fired SOFC. *ECS Trans.* 68, 1015–1022. doi: 10.1149/06801.1015ecst

Na, C. W., Woo, H.-S., Kim, H.-J., Jeong, U., Chung, J.-H., and Lee, J.-H. (2012). Controlled transformation of ZnO nanobelts into CoO/Co 3 O 4 nanowires. *CrystEngComm* 14, 3737–3741.

National Ambient Air Quality Standards by US Environmental Protection Agency (2010). *National Ambient Air Quality Standards (NAAQS) Table Has Moved*. URL: https://www.epa.gov/criteria-air-pollutants/naaqs-table.

Nielsen, J., and Hjelm, J. (2014). Impedance of SOFC electrodes: a review and a comprehensive case study on the impedance of LSM:YSZ cathodes. *Electrochim. Acta* 115, 31–45. doi: 10.1016/j.electacta.2013.10.053

Pakalapati, S., Gerdes, K., Finklea, H., Gong, M., Liu, X., and Celik, I. (2014). Micro scale dynamic modeling of LSM/YSZ composite cathodes. *Solid State Ionics* 258, 45–60. doi: 10.1016/j.ssi.2014.01.029

Simner, S. P., Anderson, M. D., Engelhard, M. H., and Stevenson, J. W. (2006). Degradation Mechanisms of La–S –Co–Fe–O3 SOFC Cathodes. *Electrochem. Solid State Lett.* 9, A478–A481. doi: 10.1149/1.2266160

Singh, P., and Birks, N. (1978). Reaction of cobalt in Ar-SO_2 atmospheres at 500-900 °C. *Oxid. Met.* 12, 23–34. doi: 10.1007/BF00609973

Upasen, S., Batocchi, P., Mauvy, F., Slodczyk, A., and Colomban, P. (2015). Chemical and structural stability of La0. 6Sr0. 4Co0. 2Fe0. 8O3- δ ceramic vs. medium/high water vapor pressure. *Ceram. Int.* 41, 14137–14147.

Wan, T. H., Saccoccio, M., Chen, C., and Ciucci, F. (2015). Influence of the Discretization Methods on the Distribution of Relaxation Times Deconvolution: implementing Radial Basis Functions with DRTtools. *Electrochim. Acta* 184, 483–499. doi: 10.1016/j.electacta.2015.09.097

Wang, C. C., Chen, K., and Jiang, S. P. (2014). Sulfur Deposition and Poisoning of La 0.6 Sr 0.4 Co 0.2 Fe 0.8 O 3-δ Cathode Materials of Solid Oxide Fuel Cells. *J. Electrochem. Soc.* 161, F1133–F1139. doi: 10.1149/2.0041412jes

Wang, C. C., Chen, K., and Jiang, S. P. (2016). Mechanism and Kinetics of SO2 Poisoning on the Electrochemical Activity of La0.8Sr0.2MnO3 Cathodes of Solid Oxide Fuel Cells. *J. Electrochem. Soc.* 163, F771–F780. doi: 10.1149/2.0221608jes

Wang, F., Kishimoto, H., Develos-Bagarinao, K., Yamaji, K., Horita, T., and Yokokawa, H. (2016). Interrelation between sulfur poisoning and performance degradation of LSCF cathode for SOFCs. *J. Electrochem. Soc.* 163, F899–F904. doi: 10.1149/2.1151608jes

Wang, C. C., O'Donnell, K., Jian, L., and Jiang, S. P. (2015). Co-deposition and poisoning of chromium and sulfur contaminants on la0.6sr0.4co0.2fe0.8o3-δ cathodes of solid oxide fuel cells. *J. Electrochem. Soc.* 162, F507–F512. doi: 10.1149/2.0231506jes

Wang, F., Yamaji, K., Cho, D. H., Shimonosono, T., Nishi, M., Kishimoto, H., et al. (2013). Evaluation of sulfur dioxide poisoning for LSCF cathodes. *Fuel Cells* 13, 520–525. doi: 10.1002/fuce.201200172

Wang, F., Yan, K., Budiman, R. A., Kishimoto, H., Ishiyama, T., Bagarinao, K. D., et al. (2020). Effect of Operating Temperature on Sulfur Distribution and Performance Degradation of Porous La0.6Sr0.4Co0.2Fe0.8O3-δ Electrode. *J. Electrochem. Soc.* 167:114507. doi: 10.1149/1945-7111/aba4e9

Yang, Y. L., Chen, C. L., Chen, S. Y., Chu, C. W., and Jacobson, A. J. (2000). Impedance Studies of Oxygen Exchange on Dense Thin Film Electrodes of La0.5Sr0.5CoO3. *J. Electrochem. Soc.* 147, 4001–4007.

Yang, Y. L., Jacobson, A. J., Chen, C. L., Luo, G. P., Ross, K. D., and Chu, C. W. (2001). Oxygen exchange kinetics on a highly oriented La0.5Sr0.5CoO3 thin film prepared by pulsed-laser deposition. *Appl. Phys. Lett.* 76, 776–778. doi: 10.1063/1.1390316

Yang, Z., Guo, M., Wang, N., Ma, C., Wang, J., and Han, M. (2017). A short review of cathode poisoning and corrosion in solid oxide fuel cell. *Int. J. Hydrogen Energy* 42, 24948–24959. doi: 10.1016/j.ijhydene.2017.08.057

Yokokawa, H. (2015). "10-Year Cooperative Investigations on Durability/Reliability of Stationary SOFCs Among Industries, Research Institutes and Universities within NEDO SOFC projects," in *11th International Conference on Ceramic Materials and Components for Energy and Environmental Applications*, (Vancouver: SOFC).

Yu, Y., Ludwig, K. F., Woicik, J. C., Gopalan, S., Pal, U. B., Kaspar, T. C., et al. (2016). Effect of Sr Content and Strain on Sr Surface Segregation of $La_{1-x}Sr_xCo_{0.2}Fe_{0.8}O_{3-\delta}$ as Cathode Material for Solid Oxide Fuel Cells. *ACS Appl. Mater. Interf.* 8, 26704–26711. doi: 10.1021/acsami.6b07118

Zubair, M., Song, R., Lee, S., Lee, J., Lim, T., and Park, S. (2014). Effect of GDC interlayer on the degradation of solid oxide fuel cell cathode during accelerated current load cycling. *Int. J. Hydrogen Energy* 39, 20799–20805. doi: 10.1016/j.ijhydene.2014.07.022

Conflict of Interest: The authors declare that the research was conducted in the absence of any commercial or financial relationships that could be construed as a potential conflict of interest.

Copyright © 2021 Hong, Anisur, Heo, Dubey and Singh. This is an open-access article distributed under the terms of the Creative Commons Attribution License (CC BY). The use, distribution or reproduction in other forums is permitted, provided the original author(s) and the copyright owner(s) are credited and that the original publication in this journal is cited, in accordance with accepted academic practice. No use, distribution or reproduction is permitted which does not comply with these terms.